Showcasing research from Professor Thomas J. Schwartz and colleagues at the Department of Chemical & Biomedical Engineering and the Forest Bioproducts Research Institute at the University of Maine, USA.

Production of jet-fuel-range molecules from biomass-derived mixed acids

A jet fuel precursor can be produced using a new process that uses biocatalysis to convert whole biomass to a mixture of organic acids which are then upgraded using heterogeneous chemical catalysis.

ROYAL SOCIETY OF **CHEMISTRY**

rsc.li/reaction-engineering

PAPER

Check for updates

Production of jet-fuel-range molecules from biomass-derived mixed acids†

Elnaz Jamalzade,[abd] Koorosh Kashkooli,[ad] Liam Griffin,[ad] G. Peter van Walsum (ID)[ad] and Thomas J. Schwartz (ID)*[acd]

Biomass has received considerable attention as a feedstock for the replacement of crude oil for producing both energy and high-value chemicals. In this work, we use a combination of chemical and biological processing to produce long-chain linear and branched ketones with low oxygen content. A mixture of medium-chain-length carboxylic acids was obtained by methane-inhibited, open-culture anaerobic fermentation of lignocellulosic biomass, and this mixture was further oligomerized using heterogeneous chemical catalysis. The products fall in the range of C_{10}–C_{20} molecules that can potentially be blended with existing hydrocarbon jet fuels. We used a Pd/CeZrO$_x$ catalyst to achieve >90% yield to C_{11+} ketones starting from C_2–C_4 mixed acids. The acids are first recovered from the fermentation broth as ethyl esters by reactive distillation using Amberlyst-45 as a catalyst. We evaluated the activity of several bifunctional catalysts for upgrading these ethyl esters into long-chain ketones, finding that 0.25 wt% Pd/CeZrO$_x$ was most active. Using a combination of experimental reaction kinetics measurements and gas-phase thermodynamics calculations, we postulate a reaction network that explains the production of the most abundant products *via* a combination of direct ester ketonization, dehydration, and hydrogenation.

Introduction

Aviation is essentially a fossil fuel industry, one which uses about 8 million barrels of oil every day.[1] The worldwide demand for jet fuel has been steadily increasing since 1980, with the consumption rate rising from 2.1m barrels per day in 1980 to 4.1m barrels per day in 2018.[2] In 2016 the International Civil Aviation Organization (ICAO) reported that 2% of global CO_2 emissions can be attributed to the aviation sector.[3] The average annual air traffic rate is projected to further increase by 4.1% per year over the period from 2015–2025, which could make the aviation industry a significant fossil-based CO_2 emitter by 2050.[3] Unlike other transportation sectors, where there might be an alternative source of energy such as renewable electricity, there is currently no way to fly nearly 8 million people every day without using the chemical potential energy stored in jet fuel molecules. Electric airplanes would require the use of heavy batteries, leading to substantial modifications to airport infrastructure and

updating of existing designs or, worse, requiring the development of entirely new airframes. So, it is crucial to find another carbon-neutral energy source that works with the current engine technology and fuel supply infrastructure. In this regard, biomass-based jet fuel is an attractive option because it provides a feasible and relatively short-term solution to decrease carbon emissions.[4,5]

There are several pathways that upgrade biomass feedstocks to jet fuel additives, many of which are available at commercial or pre-commercial scales, including the alcohol-to-jet, oil-to-jet, gas-to-jet, and sugar-to-jet processes.[6–10] The fuel closest to commercialization is hydroprocessed esters and fatty acids (HEFA).[11–13] However, the use of vegetable oils to produce HEFA fuels has led to increases in food costs in some parts of the world, and HEFA fuels are difficult to produce sustainably with high yields on a per acre basis.[14] In contrast, the sugar-to-jet pathway in particular is a flexible chemical upgrading strategy that has attracted significant attention in the last decade due to the global abundance of cellulosic biomass and the availability of several technologies to convert it to water-soluble sugars.[6,15,16] Transportation fuels must meet rigorous standards to smoothly drive engines while also maintaining engine life and suppressing harmful exhaust gas. The main components in standard of jet fuel should be C_{10}–C_{12} branched or cyclic alkanes and C_{13}–C_{16} multiply branched alkanes.[17]

In this work we apply a three-step process to convert lignocellulosic biomass to long-chain, low-oxygen species

a Department of Chemical & Biomedical Engineering, University of Maine, Orono, ME 04469, USA. E-mail: thomas.schwartz@maine.edu

b Department of Chemistry, University of Maine, Orono, ME 04469, USA

*c Frontier Institute for Research in Sensor Technology, University of Maine, Orono, ME 04469, USA*

d Forest Bioproducts Research Institute, University of Maine, Orono, ME 04469, USA

This journal is © The Royal Society of Chemistry 2021

*React. Chem. Eng.*, 2021, **6**, 845–857 | 845

containing 7–19 carbons, which are in the correct carbon-chain range to be used as jet fuel blendstocks. The first step uses open (*i.e.*, mixed) culture fermentation (OCF) for digestion of lignocellulosic biomass to produce fatty acids with chains between 4 and 8 carbons long. OCF has many advantages, including the ability to digest a variety of different organic materials including carbohydrates, proteins, and fats using enzymes made during fermentation, which adds competitive flexibility of the types of biomass feedstocks that can be upgraded.[10,18] In addition, OCF is a single-pot method, allowing for a multistep fermentation to occur in a single vessel without needing to sterilize the system, which is a significant advantage over monoculture fermentations, including ethanol production and the acetone–butanol–ethanol (ABE) process. In the second step of our process, the carboxylic-acid-rich fermentation broth undergoes acid-catalyzed esterification, where reactive distillation is used to recover and volatilize the acids while avoiding equilibrium limitations.

Because these esters are relatively short by jet-fuel standards (*e.g.*, they contain 8 or fewer carbons), the mixture of esterification products is subsequently subjected to catalytic C–C coupling to produce the long-chain species required for jet fuel applications. These reactions, shown in Scheme 1, include (a) direct ester ketonization, in which two esters react to form a linear ketone, with CO_2 and H_2O released as byproducts, (b) Claisen Dieckmann condensation/hydrogenation, in which two esters react to form a heavier, branched ketone, (c) the retro-Tischenko reaction followed by aldol condensation to produce ethanol and short-chain ketones, (d) ester hydrolysis followed by acid condensation/decarbonylation to produce a linear ketone, and (e) sequential aldol condensation/Michael addition of the linear ketones produced by (a–d) to form branched diones. The combination of reactions (a–e) yields a mixture of C_7–C_{19} linear and branched ketones and alkanes.[10] Such materials can be readily upgraded to hydrocarbon fuel blendstocks using mild hydrodeoxygenation (HDO).[19]

The reactions shown in Scheme 1 require a catalyst containing a combination of acidic sites (reactions b, d and e), basic sites (reactions a–c and e), and reduced metal sites (reactions b and c). As described in the work of Gaertner *et al.*,[20] $CeZrO_x$ contains a combination of acidic and basic functionalities that, when used as a catalyst support for a metal such as Pd, can facilitate ketonization and condensation reactions, with the Pd sites saturating C=C bonds and some C=O bonds. Consequently, in this work we evaluate whether C–C coupling of short-chain organic esters can be carried out in a single reactor system containing a Pd/$CeZrO_x$ catalyst. We show that whole biomass can be converted to compounds suitable for blending with jet fuel (following HDO) using a combination of biocatalytic processes for biomass deconstruction and defunctionalization (*i.e.*, OCF) and chemical catalytic processes for reactive separation, carbon chain elongation, and deoxygenation.
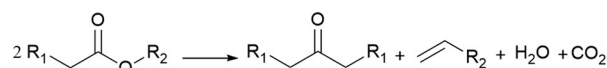
(a) Direct Ester Ketonization
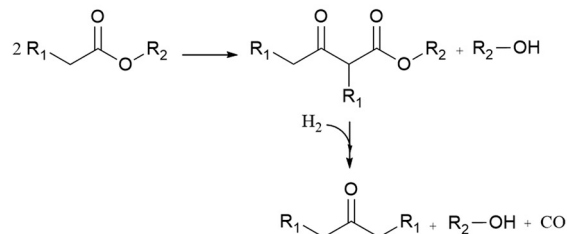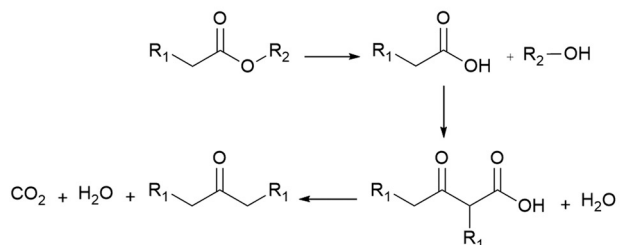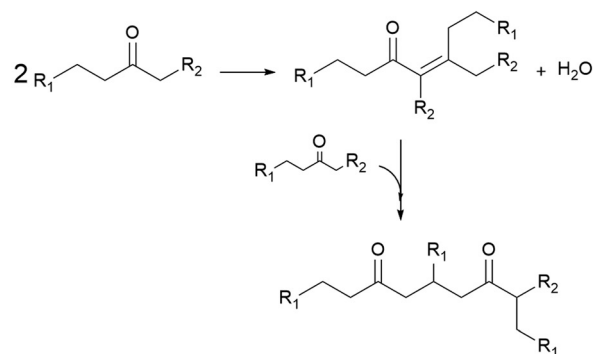
(b) Claisen Dieckmann Condensation
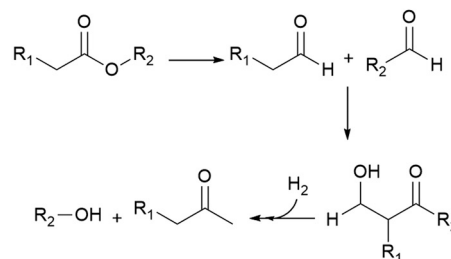
(c) Retro-Tischenko reaction followed by Aldol Condensation

(d) Hydrolysis followed by Carboxylic Acid Condensation/Decarbonylation

(e) Aldol Condensation followed by Michael Addition

Scheme 1 Catalytic reactions carried out in this work.

846 | *React. Chem. Eng.*, 2021, **6**, 845–857

This journal is © The Royal Society of Chemistry 2021

Experimental

Catalyst preparation

CeZrO$_x$ with a 1:1 Ce:Zr molar ratio was prepared by co-precipitation of nitrate precursors following the procedure described by Kunkes *et al.*[21] Briefly, aqueous solutions of Ce(NO$_3$)$_3$·6H$_2$O (Aldrich, 99.9%) and ZrO(NO$_3$)$_2$ (Alfa Aesar, 99.9%) were mixed, after which concentrated (28%) aqueous NH$_4$OH was added dropwise to raise the pH to 10, at which point a mixed carbonate material precipitated from solution. This mixed carbonate was aged at pH 10 for 3 days, after which the solids were separated by filtration, washed with ultra-pure water and ethanol, dried overnight at 373 K, and calcined in air at 623 K for 2 h to form the CeZrO$_x$ mixed oxide. The Pd/CeZrO$_x$ catalyst was prepared *via* incipient wetness impregnation (IWI) of CeZrO$_x$ with an aqueous solution of Pd(NO$_3$)$_2$ (Aldrich, 99.99%). The impregnated solid was dried overnight at 373 K and calcined in air at 623 K for 4 h. The catalyst was packed into a flow reactor and reduced at 623 K for 3 h in 50 sccm H$_2$ gas immediately prior to reaction. Synthetic hydrotalcite (Aldrich) was calcined at 773 K for 4 h to obtain a MgO–Al$_2$O$_3$ mixed oxide. The Cu/MgO–Al$_2$O$_3$ and Pd/MgO–Al$_2$O$_3$ catalysts were prepared *via* IWI of MgO–Al$_2$O$_3$ with an aqueous solution of Cu(NO$_3$)$_2$ (Aldrich, 99.99%) or Pd(NO$_3$)$_2$ (Aldrich, 99.99%), respectively. The impregnated solid was dried overnight at 373 K and calcined in air at 773 K for 4 h.[22] Prior to use, Amberlyst-45™ (Dow) was washed with 1 L deionized water (18 MΩ), dried, crushed, and sieved to less than 150 microns.

Catalyst characterization

The structure of the CeZrO$_x$ supports was verified by X-ray diffraction (XRD). A PANalytical X'PertPro diffractometer with a monochromated CuKα X-ray source was used for the diffraction studies. Diffractograms were collected over a 2θ range from 15 to 80 deg, with 0.02 deg intervals and a dwell time of 12 s.

The surface area, total pore volume, and pore size distribution of each catalyst was determined by nitrogen porosimetry measurements that were made on a Micromeritics ASAP 2020 instrument. The samples were degassed under vacuum at 473 K for 8 h to ensure the samples were thoroughly dried and free of adsorbed impurities.[23] Isotherms were measured at 77 K from $P/P_0 < 2 \times 10^{-5}$ to 0.995, spanning the micro- and meso-pore range. The surface areas were calculated according to the Brunauer–Emmett–Teller (BET) equation[24] in the relative pressure range of 0.05–0.25 (P/P_0) and the total pore volume was calculated using the Barrett–Joyner–Halenda (BJH) equation[25] corrected as described by Kruk, Jaroniec, and Sayari[26] using the adsorption branch of the N$_2$ isotherm.

Fermentation

Open culture fermentation (OCF) was carried out on lime-pretreated yellow birch wood cultured in a roller bottle apparatus held at 310 K, as described elsewhere.[27] Briefly, the pretreatment conditions for the yellow birch wood chips consisted of cooking at 10% dry solids/liquor at 423 K for 6 h with a 10% lime-to-wood ratio followed by solids particle-size-reduction achieved by grinding. The resulting solid material was supplemented with 4% chicken manure and 2% corn steep liquor as nutrient supplements, and inoculated with 4% marine organic sediment, compost, and prior fermentation broth (all wet basis), and fermented anaerobically for up to 30 days. Ethanol and/or lactic acid were added to the fermentation periodically to enhance chain elongation of the carboxylic acids and enhance the titer of medium chain-length fatty acids (MCFAs), which consisted primarily of hexanoic acid.

For the purpose of material balances, we define the digestible compounds (DC) as all the digestible carbohydrates and organic acids originating from the pretreated wood and nutrient supplements. DC does not include any supplemented ethanol and/or lactic acid added to the fermentation, nor does DC include lignin, since lignin is generally not digestible in anaerobic conditions. Digestible solids (DS) refers to the fraction of DC that is derived from the solid carbohydrates (cellulose and hemicellulose) in the feed. The material balances are done on a carbon basis, with conversions (X_i) and the MCFA selectivity (S_{MCFA}) defined as:

$$X_i = \frac{\text{Carbon in DC digested(g)} + \text{Carbon in ethanol consumed(g)}}{\text{Carbon in DC(g)} + \text{Carbon in ethanol fed(g)}}$$

(1)

$$S_{MCFA} = \frac{\text{Carbon in produced MCFAs(g)}}{\text{Carbon in DC digested(g)} + \text{Carbon in ethanol consumed(g)}}$$

(2)

Reactive distillation

The C–C coupling reactions studied here occur in the vapor phase, which necessitates recovery of the acids produced by OCF. Reactive distillation to form ethyl esters was used to accomplish both separation and volatilization, performed using a Dean–Stark apparatus (Chemglass). Hexanoic acid was chosen as a model compound to represent the mixture of acids produced by OCF. In a typical experiment, 20 mL of 30 g L^{-1} hexanoic acid (Acros Organics, 99%) in 6-undecanone solvent (TCI America, 98%), was added to a 100 mL three-necked reactor flask containing a magnetic stir bar and 0.05 g of Amberlyst 45™. The temperature of the reaction mixture was first ramped to 333 K at a rate of 33 K min^{-1}, then to 428 K at a rate of 3 K min^{-1}. The reaction mixture was stirred at 300 rpm, which was continued while a 2x molar excess of ethanol (Acros Organics, Absolute, 99.5%) was added dropwise to the reactor from an addition funnel. The reaction mixture was then held at 428 K for three hours, at which point condensation into the Dean–Stark receiver slowed significantly and the heating mantle was turned off. Once cooled, both the reaction mixture and organic product

were decanted into collection bottles for analysis by gas chromatography.

Ester oligomerization reactions

Ethyl hexanoate (Sigma-Aldrich, >99%), hydrogen (Matheson, 99.999%), and helium (Matheson, 99.999%) were all used as-purchased. The conversion of ethyl hexanoate over $CeZrO_x$, $MgO–Al_2O_3$, $Pd/CeZrO_x$, $Pd/MgO–Al_2O_3$, and $Cu/MgO–Al_2O_3$, was carried out at in a fixed bed, U-shaped reactor consisting of a quarter-inch stainless steel tube, shown schematically in Fig. 1. The catalyst was packed between two plugs of quartz wool. The reactor was heated by a well-insulated furnace. K-type thermocouples (Omega) were used to measure the reactor temperature, which was controlled by a PID controller (Automation Direct, Solo-4848) connected to a variable transformer (Staco, 3PN series). Mass flow controllers (MKS, Type 247) were used to regulate the flow of H_2 and He during the experiments. The liquid feed was pumped by a syringe pump (New Era Pump Systems, NE-1000) to a length of 1/8 inch tubing used as an evaporator, which in turn fed the reactor. A back-pressure regulator (Swagelok) was used to control the total pressure, which was measured by two gauges at the inlet and outlet of the reactor. A gas–liquid separator was submerged in an ice bath and used to collect the liquid products for analysis. The catalyst was reduced in situ at 623 K (ramp rate of 274 K min⁻¹) for 2 h in flowing H_2 (22 sccm). After the reduction was completed, the temperature and pressure were adjusted and the flow of H_2 was started. The weight hourly space velocity (WHSV) was calculated as the mass flow rate of ethyl hexanoate feed normalized by the mass of catalyst.

Analytical methods

Analysis of the fermentation products was performed using a Shimadzu high performance liquid chromatograph (HPLC) equipped with a refractive index detector (RID). Separation was achieved at 333 K using an Aminex HPX-87H column (Biorad) with an aqueous mobile phase (0.6 mL min⁻¹) buffered with 0.005 M H_2SO_4. Concentrations were determined by comparison with external standards. Carbon analysis of the inputs and outputs of the fermentation was done using a CHNO analyser (PerkinElmer).

Analysis of the liquid products of the catalytic reactions was performed with an Agilent gas chromatograph (model

7820A), equipped with an HP-5 column (30 m × 0.32 mm × 0.25 μm) and a flame ionization detector (FID). Unknown species were identified with an Agilent 7820A GC coupled to an Agilent 5975 mass selective detector (MSD). Mass spectra of unknown species were compared against standard spectra from NIST, confirmed based on the atomic mass of the molecular ion fragment and estimated retention indices based on an alkane scale. Liquid samples were collected every 24 hours. The GC program (used for both the GC/FID and GC/MSD) was as follows: helium was used as a carrier gas with a flow rate of 25 mL min⁻¹, and the inlet temperature set point was 483 K; the oven temperature was held at 373 K for 2 min then increased to 383 K at a heating rate of 275 K min⁻¹, held at 383 K for 3 min, increased to 393 K at a heating rate of 278 K min⁻¹, held at 393 K for 2 min, increased to 523 K at a heating rate of 280 K min⁻¹ and held at 523 K for 3 min; the detector temperature was set to 523 K. Quantification of each compound was determined based on a standard curve using n-butanol as an internal standard.

Fractional conversions were calculated according to eqn (3), where X represents the conversion of species i, $F_{f,i}$ represents the feed flowrate of species i, and F_i represents the molar flow rate of species i. The carbon selectivities toward reaction products, i, were calculated according to eqn (4), where S represents the selectivity and F_i represents the molar flow rate of species i, and $n_{C,i}$ represents the number of carbon atoms in species i. Mass balances typically closed to greater than 90 wt%, and carbon balances typically closed to greater than 70 mol%. Cases where the carbon balance did not fully close were due to the formation of low-concentration, minority products that could not be readily quantified. Initial selectivities were obtained by extrapolation to zero-time assuming first-order deactivation. Steady-state selectivities were obtained by averaging the first several points obtained after the reaction was observed to reach steady state, typically after approx. 48 h.

$$X_i = \left(\frac{F_{f,i} - F_i}{F_{f,i}} \right) \times 100 \qquad (3)$$

$$S_i = \left(\frac{n_{C,i} F_i}{\sum_i n_{C,i} F_i} \right) \times 100 \qquad (4)$$

Results and discussion

Fermentation

The conversion of lignocellulosic biomass to MCFAs is shown in Fig. 2. The open culture fermentation converted lime-pretreated yellow birch wood chips supplemented with chicken manure to a mixture of carboxylic acids. Fermentations were carried out in batch culture at 310 K. Intermediate metabolites included ethanol and lactic acid, which were subsequently consumed by chain elongation that yielded primarily butyric and hexanoic acids. The highest yields of MCFAs were achieved when the fermentations were
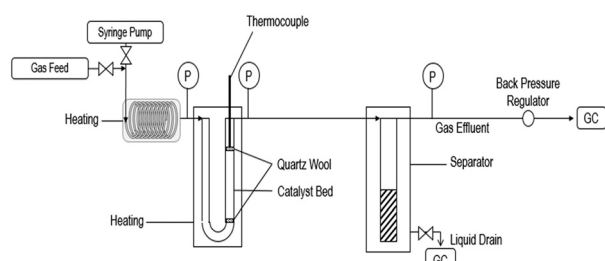

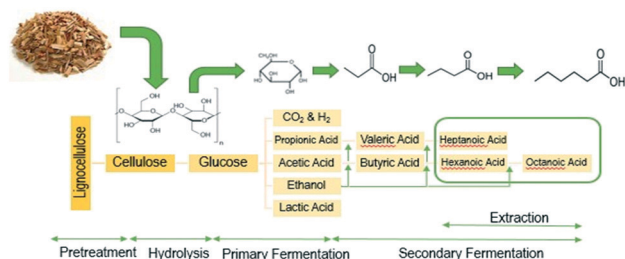Fig. 1 Schematic of the flow reactor system used for these studies.

Fig. 2 Schematic of the pretreatment and two-stage open culture fermentation process.

supplemented with ethanol and/or lactic acid. When supplemental ethanol was fed in two increments of 10 g L^{-1} to the fermenter, production of 15 g L^{-1} hexanoic acid contributed to a total MCFA titer greater than 17 g L^{-1}, achieved with 35% feedstock conversion and 41% MCFA selectivity. These fermentations also generated small amounts octanoic acid, but these were not accurately quantified by the aqueous-phase HPLC. The maximum concentration of aliphatic acids produced with lactic acid supplementation included more than 40 g L^{-1} butyric acid, up to 12 g L^{-1} propionic acid, but less than 4 g L^{-1} of hexanoic acid. Combining ethanol and lactic acid supplementation led to an elevated combination of hexanoic and butyric acids, at 14 and 7 g L^{-1} respectively. The fermentation conditions applied to generate organic acids for the esterification experiment included two ethanol supplements of 10 g L^{-1} each. To capture all the MCFAs prior to upgrading, the fermentation broth was extracted with 6-undecanone (the major primary product of C–C coupling, *vide infra*).

Material balances on the fermentation were performed on a carbon basis. Table 1 presents the carbon balance for a fermentation supplemented with ethanol doses adding up to 20 g L^{-1}.

Esterification

To identify reactive distillation conditions that lead to high yields of ethyl hexanoate from ethanol and hexanoic acid, we evaluated the effect on the ethyl hexanoate yield of the molar ratio of hexanoic acid-to-ethanol, the reactor space–time (τ), and the reaction temperature. The effect of space–time was studied by varying the catalyst loading, on a per-gram-of-feed basis, from 0.037 to 0.201 g:g of hexanoic acid, as shown in Fig. 3. As expected, increasing the space–time results in increased fractional conversion of hexanoic acid, reaching complete conversion above $\tau = 0.3$ h. The selectivity to ethyl hexanoate was 100% in all cases. Notably, when carrying out esterification of MCFAs extracted from the spent fermentation broth, some amount of catalyst inhibition was observed, indicated by the triangle (▲) in Fig. 3. While Fig. 3 reports only the conversion of hexanoic acid, the other MCFAs present in the fermentation broth were also converted to esters with 100% selectivity. The fractional conversions were as follows: $X_{C4} = 8\%$, and $X_{C6} = 58\%$. Catalyst inhibition by biogenic impurities is known to be an important problem in the catalytic conversion of biologically derived molecules.[28] For solid acid catalysts as used here, residual proteins from the fermentation can lead to deactivation by partial plugging of catalyst pores.[29] Similarly, there may also be inhibition of the acidic sites of the esterification catalyst due to amino acids that are co-extracted with the MCFAs.[30] Accordingly, we suggest that the likely reason for the lower fractional conversion of hexanoic acid here is the presence of contaminants, likely amino acids and denatured proteins, in the feed that lead to catalyst deactivation, a problem which has been previously addressed by the inclusion of polymer-derived microenvironments surrounding the active sites.[31]

Table 1 Carbon balance on wood fermentations supplemented with 20 g L^{-1} ethanol

Carbon source or product	Carbon (g)			
	Batch 3	Batch 4	Batch 5	Batch 6
Fermentation inputs				
Pretreated wood	19.85	19.85	19.85	19.85
Pretreatment liquor	1.6	1.6	1.6	1.6
Marine sediment and CSL	0.02	0.02	0.02	0.02
Manure	2.75	2.75	2.75	2.75
Fermentation inoculum	0.29	0.29	0.29	0.29
Ethanol	5.15	4.17	5.15	4.17
Total C into fermentation	29.65	28.72	29.66	28.68
Fermentation outputs				
Biotic carbon dioxide (gas)	0.51	0.46	0.78	0.86
Residual solids	22.01	22.3	21.79	20.28
Residual liquids	6.88	6.06	7.18	5.95
Liquid samples removed	0.51	0.49	0.51	0.5
Total C out of fermentation	29.91	29.3	30.25	27.59
Difference	0.26	0.58	0.59	−1.09
% error	0.88	2.02	1.99	−3.8

Batches 3 and 5 added ethanol in three doses: 10 + 5 + 5 g L^{-1}. Batches 4 and 6 added ethanol in 2 doses: 10 + 10 g L^{-1}.
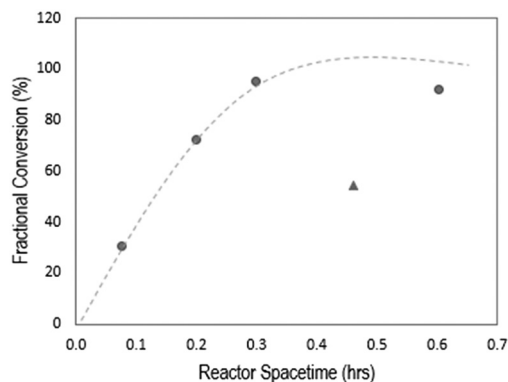
Fig. 3 Influence of reactor spacetime on fractional conversion of hexanoic acid. Spacetime was defined based on the mass of hexanoic acid in the reactor, and selectivity to ethyl hexanoate was 100% in all cases. Reaction conditions: Amberlyst 45™, 428 K, 300 rpm, 3 h, ethanol:hexanoic acid = 2:1 g:g. Hexanoic acid feed (●), fermentation broth feed (▲).

Ester oligomerization reactions

Ethyl hexanoate (**1** in Table 2) was used as a representative esterification product and was upgraded at 623 K over a Pd/CeZrO$_x$ catalyst in the presence of H$_2$. A wide range of liquid products was observed, and these are listed along with their selectivities at complete conversion in Table 3. Analysis of the gas phase revealed the presence of small amounts of ethanol,

Table 2 Products of ester oligomerization, referred to by number throughout the text

Compound	IUPAC name	#C[a]
1	Ethyl hexanoate	8
2	6-Undecanone	11
3	6-Undecanol	11
4	5-Undecene	11
5	2-Undecene	11
6	Undecane	11
7	Ethylene	2
8	1-Butene	4
9	1-Hexene	6
10	5-Ethyl-6-undecanone	13
11	Ethyl-2-butyl-3-oxooctanoate	14
12	Hexanoic acid	6
13	2-Butyl-3-oxooctanic acid	12
14	Hexanal	6
15	Acetaldehyde	2
16	3-(Hydroxymethyl)-2-heptanone	8
17	2-Heptanone	7
18	6-Tridecanone	13
19	6-Dodecanone	12
20	4-Nonanone	9
21	8-Methyl-7-tridecene-6-one	14
22	8-Methyl-6-tridecanone	14
23	12-Methyl-8-propyl-610-heptadecadione	21
24	4-Methyl-2-nonanone	10
25	2-Nonanone	9
26	8-pentadecanone	15
27	Hexadecane	16
28	4-Decanone	10

[a] Number of carbon atoms.

ethylene, and acetaldehyde but not of any significant other gas-phase organics. The behavior of the major products as a function of time-on-stream is shown in Fig. 4. Continuous reaction was performed for 30 days, with the catalyst deactivating over the first several days before stabilizing. Notably, the selectivity to **2** gradually increased during the reaction, ultimately reaching 55% after 20 days. The selectivity toward **6** decreased from 7% to 3% over the first 15 days of time-on-stream, after which it stabilized. The other major products, **17** and **3**, maintained nearly constant selectivities of 8% and 13%, respectively over the entire 30 day experiment. The remaining products are lumped by carbon-number range, and the distributions are shown in Fig. 5. The selectivity to deoxygenation products (*i.e.*, alkanes) decreases while the selectivity to C–C coupling products (*i.e.*, ketones, alcohols, *etc.*) increases over the same time range, which suggests that the Pd sites undergo deactivation during the first several days of time-on-stream, while the C–C bond-forming reactions occur mostly over sites on the CeZrO$_x$ support, which remains active.

Given that much of the reactivity described above appears to be catalyzed only by the CeZrO$_x$ support, we obtained results at the same reaction conditions (reaction temperature of 623 K, 134.9 kPa H$_2$ pressure, 135.8 kPa total pressure, and WHSV = 0.046 h^{-1}) for bulk CeZrO$_x$ without any Pd nanoparticles, the products of which are presented in Table 4. We observed 60% selectivity to **2** at steady state. The other major products were **6** and **17**, although the selectivity of **6** decreased during the course of 6 days of time-on-stream, from 18% to 8%. The selectivity to **17** was constant at *ca.* 11%. The carbon-number distributions for all products are shown in Fig. 5. Notably, the product distributions obtained both with and without Pd nanoparticles after 5 days of time-on-stream are nearly identical, confirming our hypothesis that deactivation of the Pd/CeZrO$_x$ catalyst is primarily due to loss of Pd activity.

If carbon deposition is the primary mode responsible for deactivation of the Pd sites, then decreasing the temperature (in the presence of H$_2$) may lead to an improvement in activity by favoring hydrogenation reactions *vs.* dehydrogenation. As shown in Fig. 6, the conversion unsurprisingly decreases at lower temperatures, as does the selectivity to long-chain products, possibly due to high activation barriers for C–C bond forming reactions, although we note this effect could also be due to a change in selectivity caused by decreasing the extent of reaction (*i.e.*, decreasing the conversion leads to fewer secondary and tertiary products in the series reactions). That at least some of the decrease in selectivity at low temperature is due to a decrease in the extent of reaction is supported by an observation of increased selectivity to C$_{15}$–C$_{19}$ species when 6-undecanone is fed to this catalyst at 623 K, as shown in Fig. 7, and we speculate that the decrease shown in Fig. 6 likely originates from an amalgamation of both effects. Importantly, though, the origin of the decrease in selectivity is ultimately not significant here because the lower reaction temperatures do not substantially

850 | *React. Chem. Eng.*, 2021, **6**, 845–857

This journal is © The Royal Society of Chemistry 2021

Table 3 Product distributions from the conversion of ethyl hexanoate[a]

Cmpd.	Product	#C	Initial Sel. (%)	Steady-state Sel. (%)
17	2-Heptanone	7	8	8
—	4-Methyl 3-heptanone	8	1	<1
20	4-Nonanone	9	3	1
25	2-Nonanone	9	3	2
6	Undecane	11	7	3
—	3-Ethyl 2-nonanone	11	1	1
2	6-Undecanone	11	47	55
3	6-Undecanol	11	12	13
—	Tridecane	13	<1	<1
—	2-Methyl 1-dodecanol	13	7	7
10	5-Ethyl 6-undecanone	13	1	1
18	6-Tridecanone	13	1	<1
—	6-Methyl tridecane	14	1	<1
—	6-Methyl pentadecane	16	2	2
—	6-Propyl tridecane	16	3	3
—	Nonadecane	19	1	1
—	5-Methyl octadecane	19	1	<1

[a] Reaction conditions: 0.25 wt% Pd/CeZrO$_x$, 623 K, 134.9 kPa H$_2$ pressure, 135.8 kPa total pressure, conversion 99%, and WHSV = 0.046 h^{-1}.

influence the deactivation behavior of the catalyst, suggesting that desired operation is at 623 K.

In an effort to increase the carbon numbers of the products by favoring sequential reactions, we evaluated subsequent reaction of 6-undecannone (2), which is the major product of ethyl hexanoate upgrading. To favor aldol-type condensation reactions, MgO–Al$_2$O$_3$ was selected as a catalyst because it is reported to possess not only strongly basic sites needed for C–C bond formation[32,33] but also acid–base site pairs with appropriate strength to achieve high turnover frequencies for aldol condensation (due to insertion of Al into the MgO framework).[34] Temperature-programmed desorption of CO$_2$ confirms the presence of strong base sites on this catalyst (see Fig. S3†). Using the same reaction conditions as in our previous experiments (*i.e.*, 623 K, 134.9 kPa H$_2$ pressure, 135.8 kPa total pressure, and WHSV = 0.046 h^{-1}), we again achieved complete conversion, in this case of

2. The main product was **19**, with 58% selectivity at steady state. The other major products were **4** and **17**, with 26% and 10% steady-state selectivity respectively. The selectivity distribution based on the number of carbons is shown in Fig. 7.

Following the approach of Goulas *et al.*, who observed increased aldol condensation activity for Cu and Pd supported on MgO–Al$_2$O$_3$,[35] we also evaluated Cu/MgO–Al$_2$O$_3$ and Pd/MgO–Al$_2$O$_3$ catalysts in an attempt to produce saturated, long-chain products. Cu and Pd were selected because of their high selectivity for reduction of C=O and C=C bonds, respectively. The reaction conditions were again kept the same, and the reactor was fed with **2**, with the product distributions again shown in Fig. 7. Cu/MgO–Al$_2$O$_3$ achieved >99% conversion of **2** and favored production of **4** (68% selectivity at steady state), followed by **17** (10% selectivity at steady state) and **26** (8% selectivity at steady state). Notably, we also observed the reverse reaction to
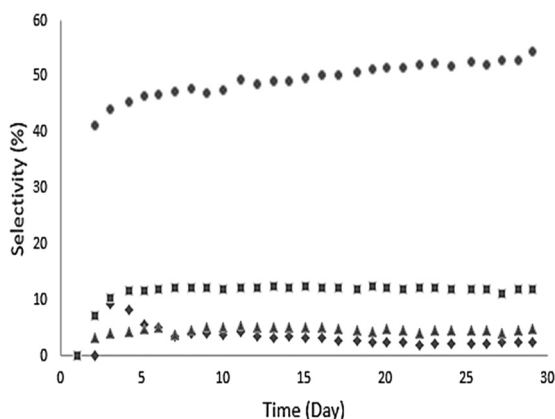
Fig. 4 Time course of selectivity to the major products of the conversion of ethyl hexanoate over 0.25 wt% Pd/CeZrO$_x$ at 623 K, 134.9 kPas H$_2$ pressure, 135.8 kPa total pressure, and WHSV = 0.046 h^{-1}. Ethyl hexanoate conversion >99%. 6-Undecanone (●), 6-undecanol (■), 2-heptanone (▲), undecane (♦).

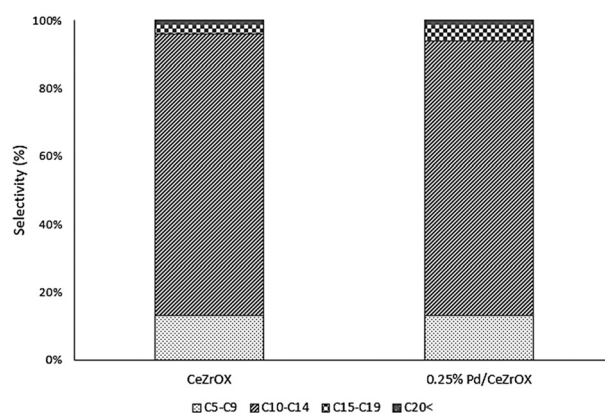**Fig. 5** Comparison of steady-state product carbon number distributions from the conversion of ethyl hexanoate over CeZrO$_x$ and 0.25 wt% Pd/CeZrO$_x$ at 623 K, 134.9 kPa H$_2$ pressure, 135.8 kPa total pressure, and WHSV = 0.046 h^{-1}.

This journal is © The Royal Society of Chemistry 2021

React. Chem. Eng., 2021, **6**, 845–857 | 851

Table 4 Product distributions from the conversion of ethyl hexanoate[a]

Cmpd.	Product	#C	Initial Sel. (%)	S.S. Sel. (%)
17	2-Heptanone	7	10	11
20	4-Nonanone	9	1	2
—	Decane	10	1	<1
6	Undecane	11	18	8
—	3-Undecene	11	1	<1
4	5-Undecene	11	4	3
2	6-Undecanone	11	56	60
3	6-Undecanol	11	1	2
—	3-Dodecene	12	<1	1
19	6-Dodecanone	12	2	1
18	6-Tridecanone	13	1	1
—	Tridecanal	13	<1	<1
—	1-Dodecanol-2-methyl	13	<1	2
—	6-Tetradecanone	14	3	4
—	6-pentadecanone	15	5	1
15	8-pentadecanone	15	<1	<1
—	1-Hexadecene	16	<1	<1
—	Tetradecanoic acid, 2-oxo-, ethyl ester	16	<1	<1
—	2-Methyl hexadecane	17	<1	<1
—	7-Heptadecanone	17	<1	1
—	1-Heptadecen-7,10-dione	17	<1	<1
—	2(3H)-Furanone, dihydro-5-tetradecyl	18	<1	<1
—	Cyclopentane, 2-hexyloctyl	19	<1	<1
—	10-Nonadecanone	19	<1	<1
—	Androstene-3á,17á-diol	19	<1	<1
—	Androstan-17-one, 3-hydroxy	19	<1	<1
—	Heptadecane, 2,6,10,15-tetramethyl	21	2	1
—	5-Methyl-6-heneicosen-11-one	22	<1	<1

[a] Reaction conditions: CeZrO$_x$ at 623 K, 134.9 kPa H$_2$ pressure, 135.8 kPa total pressure, and WHSV = 0.046 h^{-1}.

produce **1** from **2**, with *ca.* 3% selectivity to **1**. Pd/MgO–Al$_2$O$_3$ produced mostly **3** (60% selectivity at steady state), with some **17** (22% selectivity at steady state).

For comparison purposes we refer to the results of the Pd/CeZrO$_x$-catalyzed reaction as a benchmark, and all four catalysts were evaluated at identical reaction conditions. The major product obtained over Pd/CeZrO$_x$ was **4**, with 43%

selectivity at steady state selectivity, followed by **20** with 16% steady-state selectivity, and **17** with 12% steady-state selectivity. Fig. 7 compares the overall product distributions, grouped by carbon-number, for all four catalysts. The largest fraction of long-chain carbon products from **2** was obtained using Pd/CeZrO$_x$, while the smallest fraction of cracking products (*i.e.*, C$_5$–C$_9$ products) was obtained using Cu/MgO–Al$_2$O$_3$. Accordingly, we suggest that the best approach from a
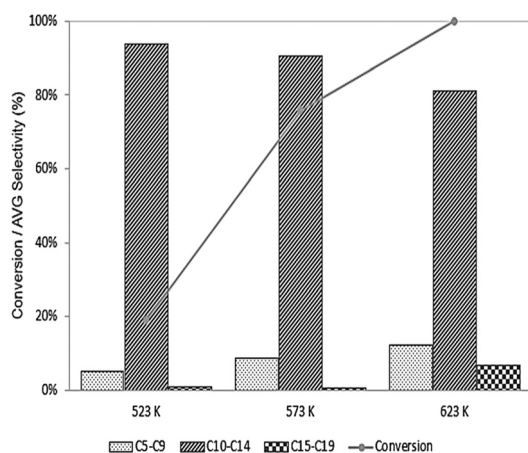

Fig. 6 The effect of the reaction temperature on the products selectivity and conversion of ethyl hexanoate over 0.25 wt% Pd/CeZrO$_x$, 134.9 kPa H$_2$ pressure, 135.8 kPa total pressure, and WHSV = 0.046 h^{-1}.

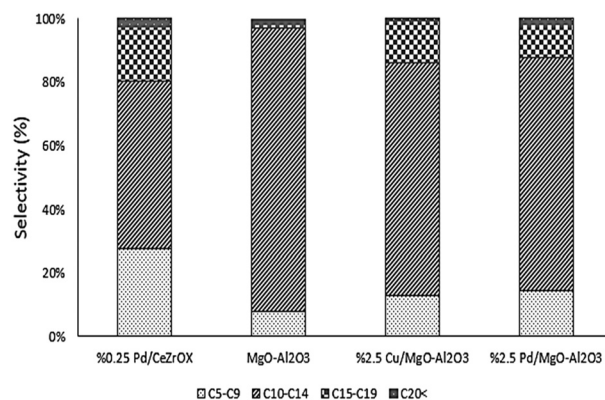**Fig. 7** Comparison of steady-state product carbon number distributions based on their carbon number from conversion of 6-undecanone over 0.25 wt% Pd/CeZrO$_x$, MgO–Al$_2$O$_3$, Cu/MgO–Al$_2$O$_3$ and Pd/MgO–Al$_2$O$_3$ at 623 K, 134.9 kPa H$_2$ pressure, 135.8 kPa total pressure, and WHSV = 0.046 h^{-1}.

852 | *React. Chem. Eng.*, 2021, **6**, 845–857

This journal is © The Royal Society of Chemistry 2021

processing standpoint for producing jet-fuel-range products is to use very low space velocities and a Pd/CeZrO$_x$ catalyst. The lighter cracking products could be recycled back into the reactor feed if needed, leading to similar oligomerization reactions as those described by Shylesh et al.[36]

Finally, to evaluate the effect of the presence of residual impurities in the fermentation broth on catalyst deactivation, we obtained results at the same reaction conditions (reaction temperature = 623 K, 135.8 kPa, and WHSV = 0.046 h^{-1}) with esterified fermentation broth over Pd/CeZrO$_x$. We also evaluated conversion of ethyl hexanoate esterified as described above as a control. The product distributions for the conversion of real fermentation broth is shown in Table 5. The conversion of **1** remained complete for both experiments. For the esterified hexanoic acid sample the main product was **6** with a steady-state selectivity of 37%. The other major products were **3** and **28** with 19% and 14% steady-state selectivities, respectively. The steady-state

selectivity distribution based on carbon numbers of products was 1% for C$_5$–C$_9$, 82% for C$_{10}$–C$_{14}$, 14% for C$_{15}$–C$_{19}$, and 4% for C$_{20+}$. The results for the control experiment were similar (see Table S1†). To assess whether impurities in the esterified broth led to catalyst deactivation, we evaluated deactivation rate constants based on the appearance of the primary product, **2**. Because we are operating at low space velocities, the product distribution is dominated by conversion of **2** to downstream products. As the catalyst deactivates, the selectivity to downstream products decreases while the selectivity to **2** increases. For simplicity, we quantified the decrease in secondary product formation based on the increase in production of **2**. Following this approach, we found a first-order deactivation rate constant of 1.4 ± 3 h^{-1} for the fermentation-derived esters, while the first-order deactivation rate constant was 0.002 ± 0.002 h^{-1} for the pure feed. That the catalyst undergoes substantial deactivation in the presence of real, biologically-derived feed is unsurprising,

Table 5 Product distributions from the conversion of esterified fermentation broth[a]

Cmpd.	Product	#C	Initial Sel. (%)	S.S. Sel. (%)
—	Nonane	9	1	<1
20	4-Nonanone	9	<1	<1
—	Decane	10	1	1
24	4-Methyl nonane	10	5	4
28	4-Decanone	10	5	14
6	Undecane	11	54	37
—	3-Methyl decane	11	<1	<1
2	6-Undecanone	11	<1	<1
3	6-Undecanol	11	<1	19
—	6-Methyl undecane	12	8	4
—	1-Hexanone 1-phenyl	12	<1	<1
—	6-Ethyl undecane	13	1	1
18	6-Tridecanone	13	<1	1
—	2-Hexyl 1-octanol	14	<1	<1
—	Tetradecane	14	1	1
—	6-Tetradecanone	14	<1	1
—	5-Methyl tetradecane	15	2	1
—	pentadecane	15	2	1
26	8-pentadecanone	15	<1	<1
—	6-Methyl pentadecane	16	2	<1
—	6-Propyl tridecane	16	<1	1
27	Hexadecane	16	1	2
—	Heptadecane	17	2	1
—	7-Methyl hexadecane	17	1	<1
—	Octadecane	18	9	4
—	2-Methyl octadecane	19	1	<1
—	Nonadecane	19	1	2
—	Eicosane	20	1	<1
—	2-Methyl eicosane	21	<1	2
—	2,6,10,15-Tetramethyl heptadecane	21	6	1
—	Docosane	22	<1	<1
—	9-Hexyl heptadecane	23	<1	<1
—	6-Methyl docosane	23	1	<1
—	Tricosane	23	<1	<1
—	2-Methyl tricosane	24	2	<1
—	Tetracosane	24	<1	<1
—	pentacosane	25	<1	<1
—	7-Hexyl eicosane	26	<1	<1
—	7-Butyl docosane	26	<1	<1
—	Heptacosane	27	<1	<1

[a] Reaction conditions: 0.25 wt% Pd/CeZrO$_x$ at 623 K, 134.9 kPa H$_2$ pressure, 135.8 kPa total pressure, and WHSV = 0.046 h^{-1}.

given the likely presence of biogenic impurities,[28] a problem that has been previously addressed by the use of polymer-derived microenvironments.[31]

Reaction network

It has previously been shown that Pd/CeZrO$_x$ catalysts contain a distribution of acidic, basic, and metallic sites,[37–43] which enable a wide range of organic chemical reactions.[21,44] Judging from the broad distribution of products generated from our experiments, it seems a complex reaction network must occur. Scheme 2 shows a potential reaction network that would explain all of the major products observed here.

The primary reaction pathway in Scheme 2 involves the self-ketonization of **1** to yield **2**, which then undergoes further hydrogenation over metal sites to yield C$_{11}$ alcohols and alkanes (**3** and **6**). As shown in *pathway A* of Scheme 2, a side product of this ketonization is ethylene, which itself can undergo oligomerization over acidic sites to yield longer-chain alkenes that can be rapidly hydrogenated to form alkanes.[45,46] As illustrated in *pathway B* in Scheme 2, **1** can also undergo a Claisen–Dieckmann condensation to produce a C$_{14}$ β-keto ester (**11**) which can convert to **2** by further hydrogenation and releasing CO and ethanol, or it can

convert to **2** by releasing CO$_2$ and ethylene. **1** can also undergo hydrolysis releasing the free acid and alcohol moieties, which react in *pathway C* of Scheme 2 by carboxylic acid condensation to produce a C$_{12}$ β-keto acid (**13**) which undergoes subsequent decarboxylation (*i.e.*, a Kagan reaction) to also yield a symmetric C$_{11}$ ketone (**2**). The ethanol released in this pathway can also form ethylene by dehydration.[47] Additionally, a C$_7$ ketone (**17**) can form by C–C cleavage (*i.e.*, the retro-Tishchenko reaction) **1**, which can be followed by further aldol condensation as shown *pathway D* of Scheme 2.[44] **17** can then undergo self-aldol condensation followed by a Michael addition of another C$_7$ ketone to form a C$_{21}$ dione (**23**). Subsequent retro-Michael C–C cleavage of this molecule leads to branched C$_{10}$ and linear C$_{11}$ ketones (**24** and **2**, respectively).[21] **17** can also react with ethanol to form a C$_9$ linear ketone (**20**)[22] or 1-butene (itself produced from oligomerization of ethylene) to form a linear C$_{11}$ ketone (**2**).[48] Furthermore, the condensation of smaller molecules can ultimately lead to longer-chain hydrocarbons; for example, the coupling of a C$_{11}$ ketone and ethylene can form a branched ketone (**10**).[49] To evaluate whether the reaction network shown in Scheme 2 is thermodynamically feasible, we obtained standard Gibbs free energy changes for each reaction using vapor-phase density functional theory (DFT)
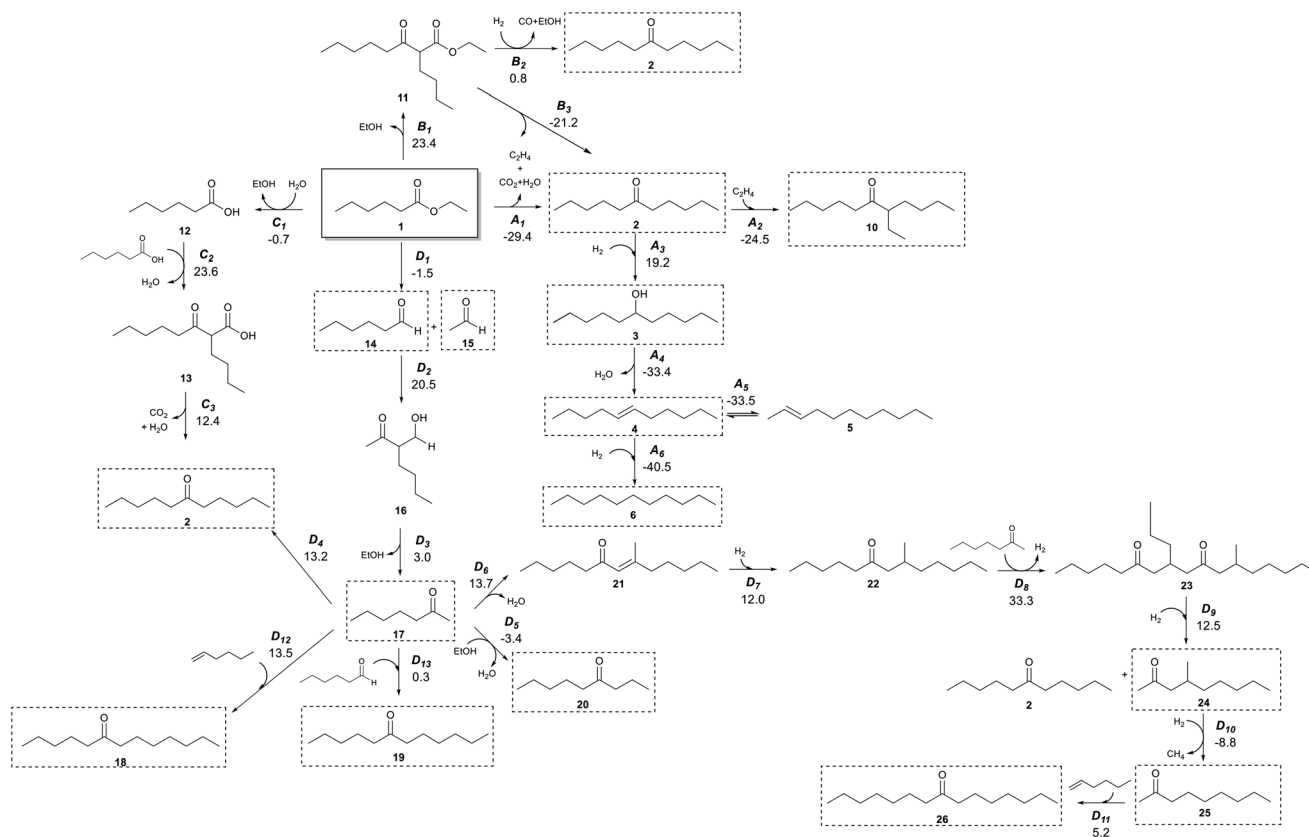
Scheme 2 Reaction network of the conversion of ethyl hexanoate with H$_2$ on Pd/CeZrO$_x$. Compound numbers in bold correspond to Table 2. Pathway labels are given in italics, with the standard Gibbs free energy change for production of each species from **1** given below in kcal mol^{-1}. For example, species **3** is produced by reaction A_3, and the standard Gibbs free energy to produce **3** from **1** is 19.2 kcal mol^{-1}. Compounds highlighted in dashed boxes were experimentally observed.

Table 6 Selectivity (%) for 6-undecanone conversion products obtained over MgO–Al$_2$O$_3$, Cu/MgO–Al$_2$O$_3$, Pd/MgO–Al$_2$O$_3$, and Pd/CeZrO$_x$[a]

Compound[b]	MgO–Al$_2$O$_3$	Cu/MgO–Al$_2$O$_3$	Pd/MgO-Al$_2$O$_3$	Pd/CeZrO$_x$
2-Heptanone	9	10	22	12
4-Nonanone	N.D.[b]	N.D.[b]	N.D.[b]	16
5-Undecanone	25	68	N.D.[b]	43
6-Dodecanone	58	N.D.[b]	60	1
8-pentadecanone	N.D.[b]	8	N.D.[b]	1

[a] Reaction conditions: 623 K, 134.9 kPa H$_2$ pressure, 135.8 kPa total pressure, and WHSV = 0.046 h^{-1}. [b] Not detected.

calculations performed with Gaussian 16.[50] The hybrid B3LYP functional was used[51] with the 6-311G(d,p) basis set. The electronic energy changes were converted to enthalpies by inclusion of zero-point energies and thermal corrections. Entropies were calculated from statistical mechanics equations using partition functions obtained from frequency calculations. Scheme 2 and Fig. S2† show the Gibbs free energy changes for each reaction at 623 K and 101 kPa. These Gibbs free energies were then used to calculate equilibrium constants for each step in the network (Table S2†) at this temperature. The major product in all reactions of **1** was **2**, which can be produced by three primary pathways, of which *pathway A* is the only one which is exergonic at these conditions.

Species **17** is observed even over catalysts that do not include Pd nanoparticles, which suggests that *pathway D* in Scheme 2 must catalyzed by basic sites on either the MgO–Al$_2$O$_3$ or CeZrO$_x$ supports. Indeed, *pathway D* leads to many of the minor products observed in our reactions, and while step D_2 is quite endergonic, the subsequent steps are quite exergonic. The low selectivity to these products would thus be unsurprising, and if the remaining activation barriers are all low, then it is reasonable to assume this pathway is responsible for production of these minority species. Notably, for the reactions with particularly small equilibrium constants, the products generally are not observed experimentally. For example, the retro-Tischenko reaction of **1** (D_1) is facile, with an equilibrium constant of 3.5, and **14** and **15** are observed as reaction products. However, the product of aldol condensation of **14** with **15** is not observed likely because of a combination between the small equilibrium constant for this reaction coupled with a low barrier for sequential decarboxylation to produce **17**, which in turn is observed experimentally. Additionally, this pathway has been observed to occur commonly on ceria-based catalysts,[44,52] and so despite the small equilibrium constants for a few steps, we suggest that the overall reaction is viable, and indeed the overall equilibrium constant for producing **17** from **1** is favorable. The presence of Pd nanoparticles facilitates C=C and C=O hydrogenation and allows for reactions according to *pathway A* in Scheme 2. This pathway is thermodynamically feasible (see Table S2†), and we accordingly observe production of **3**, **4**, and **6** starting from **2** for catalysts containing Pd and, to a lesser extent, Cu (see Table S2†). Interestingly, for unpromoted CeZrO$_x$ we also observe small amounts of **4** and **6**, although we do not see

substantial production of **3**. These saturated species could be produced *via* transfer hydrogenation as described by Vivier *et al.*[52]

To identify the potential for base-catalyzed coupling of ketones, we studied the conversion of **2** over Pd/CeZrO$_x$ and Pd/MgO–Al$_2$O$_3$ (Table 6), which led to species **17** and **8**, likely by the reverse of *pathway D* (Scheme 2), with an equilibrium constant of 10^{-5}, which is thermodynamically feasible based on the argument presented above. Both **1** and **14** were detected in the product mixture, further suggesting that *pathway D* is reversible. Species **19** can also be obtained *via* *pathway D*, by condensation of **14** and **17**. Notably, significant amounts of **19** are only observed for MgO–Al$_2$O$_3$-based catalysts, suggesting that stronger base sites are needed for the aldol condensation of **14** and **17**.

Conclusions

In summary, we have applied a three-step process to convert lignocellulosic biomass to species containing between 7 and 19 carbons, which are in the correct carbon-chain range to be used as jet fuel blendstocks following mild HDO. The first step uses open culture fermentation (OCF) for digestion of lignocellulosic biomass to produce fatty acids with chains between 4 and 8 carbons long. In the second step of our process, the carboxylic-rich fermentation broth undergoes acid-catalyzed esterification, where reactive distillation is used to avoid equilibrium limitations. The mixture of esterification products is subsequently subjected to catalytic C–C coupling to produce longer chain molecules required for jet fuel applications. We have achieved >99% conversion of a model feedstock (ethyl hexanoate) into a wide range of C$_7$–C$_{19}$ molecules using bifunctional metal/mixed-oxide catalysts. In particular, we found that Pd/CeZrO$_x$ is highly selective and stable under reaction conditions. Of the products detected using this catalyst, more 90 mol% are C$_{11}$ or greater compounds that contain little oxygen and would be appropriate for blending with jet fuel. These species are present as aliphatic alcohols, aldehydes, and ketones, all of which can be reduced to form hydrocarbons by simple treatment with an alumina-supported bimetallic catalyst system (*e.g.*, Pd–Ni and Pd–Fe) at moderate temperatures, as described by Lee, *et al.*[53]

The catalyst was largely stable with respect to time-on-stream for at least 30 days, with small decreases in the selectivity to deoxygenation products (*i.e.*, alkanes), while the

This journal is © The Royal Society of Chemistry 2021

React. Chem. Eng., 2021, **6**, 845–857 | **855**

selectivity to C–C coupling products (*i.e.*, ketones, alcohols, *etc.*) increases over the same time range. This trend suggests that the Pd sites on the catalyst can undergo deactivation during the first several days of time-on-stream, while the C–C bond-forming reactions occur mostly over sites on the CeZrO$_x$ support, which remains fully active.

In an effort to increase the carbon numbers of the products by favoring sequential reactions, we evaluated subsequent reaction of 6-undecannone (**2**) over Pd/CeZrO, MgO–Al$_2$O$_3$,Cu/MgO–Al$_2$O$_3$ and Pd/MgO–Al$_2$O$_3$, and the use of MgO–Al$_2$O$_3$ catalysts showed no advantages over CeZrO$_x$ catalysts in this study. Finally, we postulated a reaction network that accounts for the major products observed in this work and verified that the reaction network is thermodynamically feasible.

Conflicts of interest

There are no conflicts to declare.

Acknowledgements

References

1   B. Sharafedin, T. Hepher and K. Samanta, *Jet fuel demand to remain low as airlines buckle up for tough ride*, https://www.reuters.com/article/us-global-oil-jet-fuel/jet-fuel-demand-to-remain-low-as-airlines-buckle-up-for-tough-ride-idUSKCN21X1DS, (accessed October 10, 2020).

2   U.S. Energy Information Administration (EIA) - Qb, https://www.eia.gov/opendata/qb.php?sdid=INTL.63-2-WORL-TBPD.A.

3   E. Terrenoire, D. A. Hauglustaine, T. Gasser and O. Penanhoat, *Environ. Res. Lett.*, 2019, **14**(8), 084019.

4   T. J. Schwartz, A. R. P. van Heiningen and M. C. Wheeler, *Green Chem.*, 2010, **12**, 1353–1356.

5   P. A. Case, A. R. P. van Heiningen and M. C. Wheeler, *Green Chem.*, 2012, **14**, 85–89.

6   W. C. Wang and L. Tao, *Renewable Sustainable Energy Rev.*, 2016, **53**, 801–822.

7   M. Crocker, *Thermochemical Conversion of Biomass to Liquid Fuels and Chemicals*, Royal Society of Chemistry, 2010.

8   D. R. Shonnard, L. Williams and T. N. Kalnes, *Environ. Prog. Sustainable Energy*, 2010, **28**, 382–392.

9   D. Klein-Marcuschamer, P. Oleskowicz-Popiel, B. A. Simmons and H. W. Blanch, *Biotechnol. Bioeng.*, 2012, **109**, 1083–1087.

10   H. N. Chang, N. J. Kim, J. Kang and C. M. Jeong, *Biotechnol. Bioprocess Eng.*, 2010, **15**, 1–10.

11   J. Han, A. Elgowainy, H. Cai and M. Q. Wang, *Bioresour. Technol.*, 2013, **150**, 447–456.

12   P. Gegg, L. Budd and S. Ison, *J. Air Transp. Manag.*, 2014, **39**, 34–40.

13   A. Milbrandt, C. Kinchin and R. McCormick, *The Feasibility of Producing and Using Biomass-Based Diesel and Jet Fuel in the United States*, 2013.

14   J. Janaun and N. Ellis, *Renewable Sustainable Energy Rev.*, 2010, **14**, 1312–1320.

15   H. Olcay, A. V. Subrahmanyam, R. Xing, J. Lajoie, J. A. Dumesic and G. W. Huber, *Energy Environ. Sci.*, 2013, **6**, 205–216.

16   J. Han, L. Tao and M. Wang, *Biotechnol. Biofuels*, 2017, **10**, 1–15.

17   Y. Nakagawa, M. Tamura and K. Tomishige, *Fuel Process. Technol.*, 2019, **193**, 404–422.

18   H. W. B. Daniel Klein-Marcuschamer, P. Oleskowicz-Popiel and B. A. Simmons, *Biotechnol. Bioeng.*, 2011, **109**, 1083–1087.

19   G. W. Huber, S. Iborra and A. Corma, *Chem. Rev.*, 2006, **106**, 4044–4098.

20   C. A. Gaertner, J. C. Serrano-Ruiz, D. J. Braden and J. A. Dumesic, *Ind. Eng. Chem. Res.*, 2010, **49**, 6027–6033.

21   E. L. Kunkes, E. I. Gürbüz and J. A. Dumesic, *J. Catal.*, 2009, **266**, 236–249.

22   K. A. Goulas, G. Gunbas, P. J. Dietrich, S. Sreekumar, A. Grippo, J. P. Chen, A. A. Gokhale and F. D. Toste, *ChemCatChem*, 2017, **9**, 677–684.

23   R. A. Pollock, B. R. Walsh, J. Fry, I. T. Ghampson, Y. B. Melnichenko, H. Kaiser, R. Pynn, W. J. Desisto, M. C. Wheeler and B. G. Frederick, *Chem. Mater.*, 2011, **23**, 3828–3840.

24   S. Brunauer, P. H. Emmett and E. Teller, *J. Am. Chem. Soc.*, 1938, **60**, 309–319.

25   E. P. Barrett, L. G. Joyner and P. P. Halenda, *J. Am. Chem. Soc.*, 1951, **73**, 373–380.

26   M. Kruk, M. Jaroniec and A. Sayari, *Langmuir*, 1997, **13**, 6267–6273.

27   K. Kashkooli, *MS Thesis*, University of Maine, 2019.

28   T. J. Schwartz, B. J. O'Neill, B. H. Shanks and J. A. Dumesic, *ACS Catal.*, 2014, **4**, 2060–2069.

29   Z. Zhang, J. E. Jackson and D. J. Miller, *Bioresour. Technol.*, 2008, **99**, 5873–5880.

30   R. Luque, C. S. K. Lin, C. Du, D. J. Macquarrie, A. Koutinas, R. Wang, C. Webb and J. H. Clark, *Green Chem.*, 2009, **11**, 193–200.

31   T. J. Schwartz, R. L. Johnson, J. Cardenas, A. Okerlund, N. A. Da Silva, K. Schmidt-Rohr and J. A. Dumesic, *Angew. Chem., Int. Ed.*, 2014, **53**, 12718–12722.

32   A. Corma, V. Fornés, R. M. Martín-Aranda and F. Rey, *J. Catal.*, 1992, **134**, 58–65.

33   D. Tichit, M. H. Lhouty, A. Guida, B. H. Chiche, F. Figueras, A. Auroux, D. Bartalini and E. Garrone, *J. Catal.*, 1995, **151**, 50–59.

34   J. T. Kozlowski and R. J. Davis, *ACS Catal.*, 2013, **3**, 1588–1600.

856 | *React. Chem. Eng.*, 2021, **6**, 845–857

This journal is © The Royal Society of Chemistry 2021

35 K. A. Goulas, S. Sreekumar, Y. Song, P. Kharidehal, G. Gunbas, P. J. Dietrich, G. R. Johnson, Y. C. Wang, A. M. Grippo, L. C. Grabow, A. A. Gokhale and F. D. Toste, *J. Am. Chem. Soc.*, 2016, **138**, 6805–6812.

36 S. Shylesh, D. Kim, A. A. Gokhale, C. G. Canlas, J. O. Struppe, C. R. Ho, D. Jadhav, A. Yeh and A. T. Bell, *Ind. Eng. Chem. Res.*, 2016, **55**, 10635–10644.

37 L. F. Liotta, G. Pantaleo, A. Macaluso, G. Marcì, S. Gialanella and G. Deganello, *J. Sol-Gel Sci. Technol.*, 2003, **28**, 119–132.

38 M. Glorius, M. A. C. Markovits and C. Breitkopf, *Catalysts*, 2018, **8**, 1–25.

39 K. Otsuka, Y. Wang and M. Nakamura, *Appl. Catal., A*, 1999, **183**, 317–324.

40 J. C. Serrano-Ruiz, J. Luettich, A. Sepúlveda-Escribano and F. Rodríguez-Reinoso, *J. Catal.*, 2006, **241**, 45–55.

41 S. M. de Lima, A. M. Silva, U. M. Graham, G. Jacobs, B. H. Davis, L. V. Mattos and F. B. Noronha, *Appl. Catal., A*, 2009, **352**, 95–113.

42 F. Al-Wadaani, E. F. Kozhevnikova and I. V. Kozhevnikov, *J. Catal.*, 2008, **257**, 199–205.

43 S. M. de Lima, I. O. da Cruz, G. Jacobs, B. H. Davis, L. V. Mattos and F. B. Noronha, *J. Catal.*, 2008, **257**, 356–368.

44 R. Kumar, N. Enjamuri, S. Shah, A. S. Al-Fatesh, J. J. Bravo-Suárez and B. Chowdhury, *Catal. Today*, 2018, **302**, 16–49.

45 P. Cossee, *J. Catal.*, 1964, **3**, 80–88.

46 S. Moussa, P. Concepción, M. A. Arribas and A. Martínez, *ACS Catal.*, 2018, **8**, 3903–3912.

47 R. Klimkiewicz, H. Grabowska and L. Syper, *Kinet. Catal.*, 2003, **44**, 283–286.

48 C. Y. Ho, K. D. Schleicher, C. W. Chan and T. F. Jamison, *Synlett*, 2009, **2009**, 2565–2582.

49 F. Mo and G. Dong, *Science*, 2014, **345**, 68–72.

50 M. J. Frisch, G. W. Trucks, H. B. Schlegel, G. E. Scuseria, M. A. Robb, J. R. Cheeseman, G. Scalmani, V. Barone, G. A. Petersson, H. Nakatsuji, X. Li, M. Caricato, A. V. Marenich, J. Bloino, B. G. Janesko, R. Gomperts, B. Mennucci, H. P. Hratchian, J. V. Ortiz, A. F. Izmaylov, J. L. Sonnenberg, D. Williams-Young, F. Ding, F. Lipparini, F. Egidi, J. Goings, B. Peng, A. Petrone, T. Henderson, D. Ranasinghe, V. G. Zakrzewski, J. Gao, N. Rega, G. Zheng, W. Liang, M. Hada, M. Ehara, K. Toyota, R. Fukuda, J. Hasegawa, M. Ishida, T. Nakajima, Y. Honda, O. Kitao, H. Nakai, T. Vreven, K. Throssell, J. A. Jr., J. E. Peralta, F. Ogliaro, M. J. Bearpark, J. J. Heyd, E. N. Brothers, K. N. Kudin, V. N. Staroverov, T. A. Keith, R. Kobayashi, J. Normand, K. Raghavachari, A. P. Rendell, J. C. Burant, S. S. Iyengar, J. Tomasi, M. Cossi, J. M. Millam, M. Klene, C. Adamo, R. Cammi, J. W. Ochterski, R. L. Martin, K. Morokuma, O. Farkas, J. B. Foresman and D. J. Fox, *Gaussian 16 (Revision B.01)*, Gaussian, Inc., Wallingford CT, 2016.

51 C. Lee, W. Yang and R. G. Parr, *Phys. Rev. B*, 1988, **37**, 785–789.

52 L. Vivier and D. Duprez, *ChemSusChem*, 2010, **3**, 654–678.

53 J. Lee, Y. T. Kim and G. W. Huber, *Green Chem.*, 2014, **16**, 708–718.

This journal is © The Royal Society of Chemistry 2021

React. Chem. Eng., 2021, **6**, 845–857 | **857**